

# We are IntechOpen, the world's leading publisher of Open Access books Built by scientists, for scientists

6,900

Open access books available

186,000

International authors and editors

200M

Downloads

Our authors are among the

154

Countries delivered to

TOP 1%

most cited scientists

12.2%

Contributors from top 500 universities



WEB OF SCIENCE™

Selection of our books indexed in the Book Citation Index  
in Web of Science™ Core Collection (BKCI)

Interested in publishing with us?  
Contact [book.department@intechopen.com](mailto:book.department@intechopen.com)

Numbers displayed above are based on latest data collected.  
For more information visit [www.intechopen.com](http://www.intechopen.com)



---

# **Obstacle Avoidance Task for a Wheeled Mobile Robot – A MATLAB-Simulink-Based Didactic Application**

---

R. Silva-Ortigoza, C. Márquez-Sánchez,  
F. Carrizosa-Corral, V. M. Hernández-Guzmán,  
J. R. García-Sánchez, H. Taud,  
M. Marciano-Melchor and J. A. Álvarez-Cedillo

Additional information is available at the end of the chapter

<http://dx.doi.org/10.5772/58392>

---

## **1. Introduction**

In recent years, the development of wheeled mobile robots (WMR) has allowed for significant progress in various fields of science due to the wide scope of applications in which such robots can be employed [1]. These fields include medical assistance, space and marine exploration, leisure, entertainment, technology research and development, metal-mechanics and chemical industries, military research, cleaning in diverse surroundings, agriculture, inspection, security, and transportation, among others. The discussion regarding mobile robotics has been undergoing a slowly-evolving transition and continues even now to be a topic of great interest at the international level.

Mobile robots can be classified according to their locomotion method into three types [1]: wheeled, legged, and caterpillar track. Although both legged and caterpillar track locomotion have been widely researched, most mobile robots that have been built, evaluated, and reported use wheels to move. This reflects their increasing use in applications such as planetary exploration, mining, inspection, security, rescue operations, hazardous waste clean-up, and medical assistance. A review associated with WMR can be found in [1]; although much of the research that has been carried out thus far has provided a significant contribution to the topic, the development and conception of a mobile robot that has total autonomy of operation remains a distant prospect.

In order to improve the autonomy of mobile robots, experiments examining control have generally focused on solving the following problems: (1) mobile robot positioning,

(2) stabilization, (3) trajectory tracking control, (4) trajectory planning, and (5) obstacle avoidance. In this respect, significant progress (albeit not total) has been achieved. The present work focuses on the obstacle avoidance problem, whose objective is providing a mobile robot with collision-free navigation through a workspace in which obstacles have been predeterminedly distributed. In particular, we develop, step-by-step, a MATLAB-Simulink application that describes the experimental implementation of a WMR controller which allows collision-free navigation.

According to the robotics literature, a variety of different methods are available with which to perform the obstacle avoidance task, the most relevant being: edge detection [2], cell decomposition [3], map building [4], and artificial potential fields [5]; a description of all of these methods can be found in [1], with the artificial potential field method notably the most cited. In the present work the artificial potential field technique is employed to carry out an obstacle avoiding task with a WMR. Developed by Khatib [5], in this method the mobile robot can be considered as a particle, the obstacles presented within the workspace as particles that exert a repulsive force on the mobile robot, and the goal as a particle that exerts an attractive force on the mobile robot. Thus, a resultant potential field is achieved that leads the trajectory that the mobile robot must follow in order to evade the obstacles –which might be considered previously in the method, or else detected via a sensor– and reach the goal. It is worth mentioning that applying the artificial potential field method does not require a great deal of computational complexity because it is based on the implementation of mathematical functions representing the attractive and repulsive forces exerted on the mobile robot. Finally, since the initial establishment of the artificial potential field method, a number of different modifications and implementations have been developed in conjunction with other techniques. Hence, some variations of the method have been reported in [6–13].

Whereas the works cited above introduce research examining the obstacle avoidance task using the artificial potential field method with WMRs, the present document describes the step-by-step experimental implementation of a hierarchical control which is performed along with the artificial potential field method in carrying out the obstacle avoidance task with the differentially-driven WMR built and reported in [14]. This work is aimed at helping students integrate theoretical and practical knowledge through the use of a relevant and modern open-architecture testbed that allows rapid prototyping [15]. On the one hand, simulations are carried out using MATLAB-Simulink. On the other hand, MATLAB Simulink, ControlDesk, and the DS1104 electronic board (dSPACE) are employed for the real-time experiments since the graphical environment provided by Simulink facilitates the analysis, design, and construction of dynamic systems.

The present work is structured as follows. Section 2 describes the basis of the artificial potential field method for the obstacle avoidance task. The hierarchical control applied to the WMR in performing the obstacle avoidance task is detailed in Section 3. In Section 4, a description of the block diagrams programmed in MATLAB Simulink, along with the simulation results associated with the closed-loop system, are presented. The subsystems of the prototype employed are then described in Section 5, with Section 6 containing a description of the blocks developed in MATLAB-Simulink for the experimental implementation of the hierarchical control via MATLAB-Simulink, ControlDesk, and the DS1104 in the prototype. Finally, conclusions drawn from the study are presented in Section 7.

## 2. Artificial potential field

This section describes the artificial potential field method, which in conjunction with a controller allows the accomplishment of the obstacle avoidance task. Although the method has been modified by various authors in order to solve some of its inherent problems, these modifications account for individual problems separately and not necessarily in an optimal manner. Therefore, the classic method is employed herein. The artificial potential field method consists of the creation of artificial potential fields, with the goal being the development of an attractive pole and obstacles acting as repulsive surfaces for the mobile robot. Whereas the attractive force produced by the artificial potential field associated with the goal generates a continuous trajectory towards it, the repulsive force produced by the fields associated with the obstacles move the mobile robot away from them. When combining both forces a third force is produced which enables an effective control. It is worth noting that when the attractive and repulsive forces are equal in magnitude and opposite in orientation, as generated by a specific goal and obstacle distribution, the mobile robot cannot accomplish the obstacle avoidance task. When this occurs, the mobile robot is said to be trapped within a local minimum.

The present study addresses a problem involving a WMR, an obstacle, and the goal which is directly extendable to the general case, namely, the  $n$  obstacles problem. Consider a bidimensional workspace and a fixed coordinate system  $X$ - $Y$  in which the coordinates of a point associated with the WMR are determined by  $q = (x_1, y_1)$  (see Figure 4), the obstacle by  $q_{obs} = (x_o, y_o)$ , and the goal by  $q_m = (x_m, y_m)$ . Moreover, suppose that the obstacle and the goal separately exert a force on the WMR, generating a resultant force,  $F_{total}$ , given by

$$F_{total} = F_{at}(q) + F_{rep}(q), \quad (1)$$

where  $F_{at}(q)$  is the attractive force produced by the goal and  $F_{rep}(q)$  is the repulsive force generated by the obstacle.

The resultant force is considered to be exerted by an artificial potential field determined by

$$U(q) = U_{at}(q) + U_{rep}(q), \quad (2)$$

with  $U_{at}(q)$  and  $U_{rep}(q)$  being the artificial potential fields associated with the goal and the obstacle, respectively, where

$$F_{at}(q) = -\nabla U_{at}(q), \quad (3)$$

$$F_{rep}(q) = -\nabla U_{rep}(q), \quad (4)$$

and the operator  $\nabla$  is defined as  $\left(\frac{\partial}{\partial x}, \frac{\partial}{\partial y}\right)$ . The attractive and repulsive forces are represented by the negative gradient of the potential fields, as expressed in (3) and (4). Hence, depending on the positions of the obstacle and the goal, the resultant force will lead the mobile robot's point  $q$ , collision-free, towards the goal.

## 2.1. Attractive potential

One of the most commonly-used attractive potential fields was presented in [16], and is determined by

$$U_{at}(q) = \frac{1}{2}\xi\rho^k(q, q_m), \quad (5)$$

where  $\xi$  is a positive scale factor,  $q$  is the mobile robot's reference point,  $q_m$  is the goal's coordinate,  $\rho(q, q_m) = \|q - q_m\|$  is the distance between  $q$  and  $q_m$ , and  $k = 1, 2$ .

- For  $k = 1$ , the attractive potential field presents a conic shape, as shown in Figure 1. The attractive force generated by  $U_{at}$  has constant amplitude except at the goal, where  $U_{at}$  is non-differentiable, as given by

$$F_{at}(q) = -\nabla U_{at}(q) = -\frac{1}{2}\xi \frac{(q - q_m)}{\|q - q_m\|}. \quad (6)$$

- For  $k = 2$ , the attractive potential field presents a parabolic shape, as shown in Figure 2. The corresponding attractive force is determined by the negative gradient of the attractive potential, i.e.,

$$F_{at}(q) = -\nabla U_{at}(q) = -\xi(q - q_m), \quad (7)$$

which converges linearly to zero as the mobile robot approaches the goal.

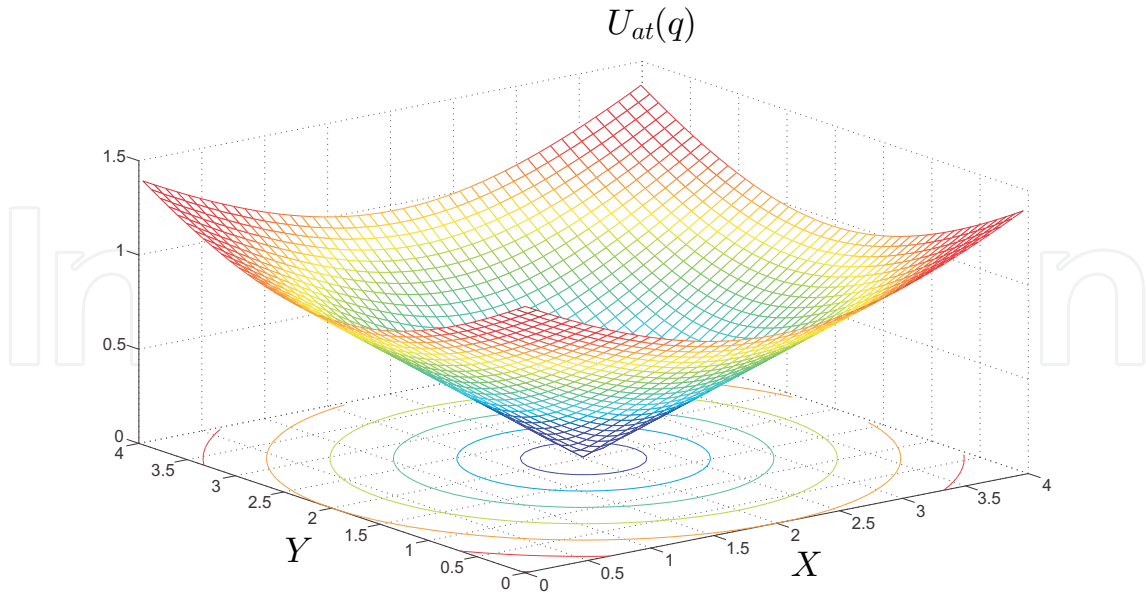


**Figure 1.** Attractive potential field for  $k = 1$ .

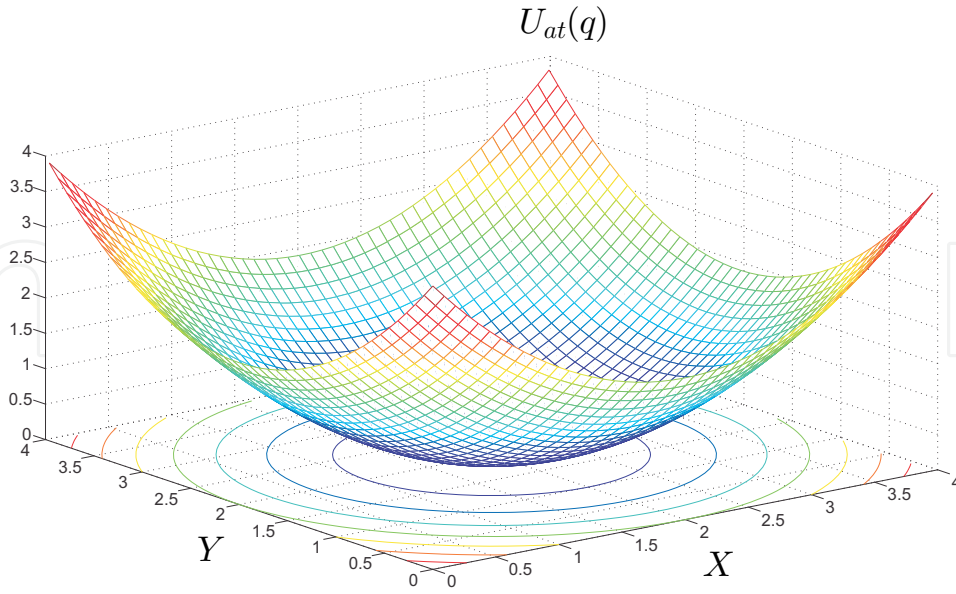


**Figure 2.** Attractive potential field for  $k = 2$ .

## 2.2. Repulsive potential

One commonly-used repulsive potential function takes the following form [16]:

$$U_{rep}(q) = \begin{cases} \frac{1}{2}\eta \left[ \frac{1}{\rho(q, q_{obs})} - \frac{1}{\rho_0} \right]^2, & \text{for } \rho(q, q_{obs}) \leq \rho_0, \\ 0, & \text{for } \rho(q, q_{obs}) > \rho_0, \end{cases} \quad (8)$$

where  $\eta$  is a positive scale factor,  $\rho(q, q_{obs}) = \|q - q_{obs}\|$  is the shortest distance between the mobile robot and the obstacle, and  $\rho_0$  is a positive constant that represents the distance of the obstacle's influence. The graphical representation associated with the obstacle defined by (8) is shown in Figure 3. Hence, the repulsive force,  $F_{rep}(q)$ , associated with (8), is determined by

$$F_{rep}(q) = -\nabla U_{rep}(q) = \begin{cases} \eta \left[ \frac{1}{\rho(q, q_{obs})} - \frac{1}{\rho_0} \right] \frac{q - q_o}{\rho^3(q, q_{obs})}, & \text{for } \rho(q, q_{obs}) \leq \rho_0, \\ 0, & \text{for } \rho(q, q_{obs}) > \rho_0. \end{cases} \quad (9)$$

Finally, it is worth mentioning that the described artificial potential field method depends upon the relative position of the mobile robot to the obstacle, unlike other methods such as that of Krogh [17] in which the potential field is sensitive to the impact time. Furthermore, implementing the presented method requires knowledge of the coordinates of the mobile robot, the obstacle, and the goal, i.e.,  $q = (x_1, y_1)$ ,  $q_{obs} = (x_o, y_o)$ , and  $q_m = (x_m, y_m)$ , respectively. In the present work, it is assumed that these coordinates are already known; nevertheless, the employed method can also be extended to sensors that allow the acquisition of these coordinates in real-time.

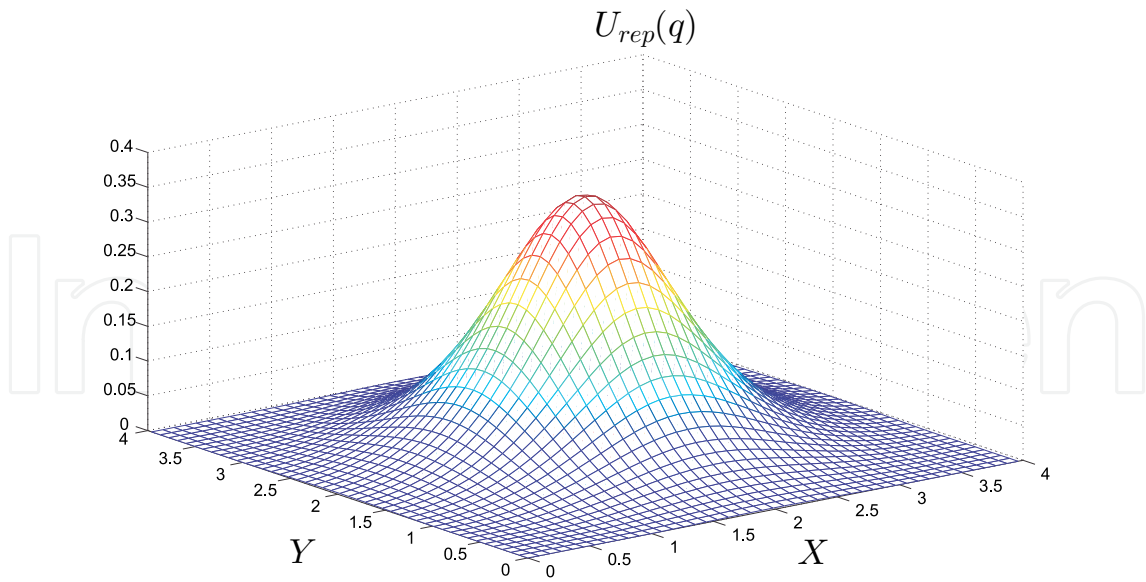


**Figure 3.** Repulsive potential field.

### 3. Control for obstacle avoidance of WMR

This section presents the hierarchical control developed in [18], and analyzed in [26] for a trailer-like vehicle. Using the kinematic model associated with the differentially-driven WMR, an input-output linearization control is proposed that, in conjunction with the artificial potential field method, enables the accomplishment of the obstacle avoidance task. A PI control is then proposed for each DC motor, allowing the WMR to move. Finally, with the ultimate aim of experimentally accomplishing the obstacle avoidance task with a WMR prototype, a hierarchical control is proposed which merges the said controls, similar to the structure presented in [14, 19–23].

#### 3.1. Control of the kinematic model

The mobile robot under study is a vehicle comprising two traction wheels, left and right. These two wheels are identical, parallel to each other, non-deformable, and joined by a shaft. The robot also comprises two omnidirectional wheels, front and rear, that ensure the robot platform remains on a plane. Supposing movement is restricted on an  $XY$  plane and that there is no wheel slip, existing literature (see [24]) describe the WMR kinematics as given by

$$\begin{aligned}\dot{x} &= \frac{(\omega_r + \omega_l) r}{2} \cos \varphi, \\ \dot{y} &= \frac{(\omega_r + \omega_l) r}{2} \sin \varphi, \\ \dot{\varphi} &= \frac{(\omega_r - \omega_l) r}{2l},\end{aligned}\tag{10}$$

where  $(x, y)$  denotes the position of the mid-point of the shaft that joins the wheels,  $\varphi$  is the angle formed by the WMR symmetry axis and the positive  $X$ -axis,  $\omega_r$  and  $\omega_l$  are the

angular velocities of the right and left wheels, respectively,  $r$  is the wheel ratio, and  $2l$  is the separation between the wheels. Parameters and variables associated with the WMR are shown in Figure 4. This WMR configuration is known as differential traction.

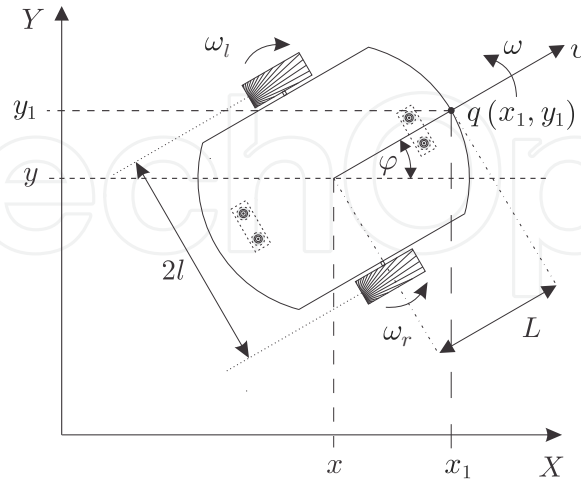


**Figure 4.** WMR diagram.

Whereas the derivative with respect to time  $t$ , associated with the state variables, is denoted by a dot in equations (10) and (12), in the rest of the chapter it is represented explicitly, i.e.,  $\frac{d}{dt}$ .

Since the mathematical model described by (10) presents a noninvertible relationship between the controls,  $(\omega_r, \omega_l)$ , and the outputs,  $(x, y)$ , it is not possible to propose a control via input-output linearization. For simplicity, another reference point associated with the WMR that can therefore be considered is the front part which has the coordinates  $q = (x_1, y_1)$  (see Figure 4). The coordinates of  $q$  expressed in terms of  $x, y$ , and  $\varphi$  are determined by

$$\begin{aligned} x_1 &= x + L \cos \varphi, \\ y_1 &= y + L \sin \varphi, \end{aligned} \quad (11)$$

where  $L$  is the distance from the mid-point of the wheel shaft,  $(x, y)$ , to the point  $q$  in the direction perpendicular to the shaft. Deriving system (11) with respect to time obtains the WMR kinematic model associated with point  $q = (x_1, y_1)$ , which is given by

$$\begin{pmatrix} \dot{x}_1 \\ \dot{y}_1 \end{pmatrix} = A(\varphi) \begin{pmatrix} \omega_r \\ \omega_l \end{pmatrix}, \quad (12)$$

with

$$A(\varphi) = \begin{pmatrix} \cos \varphi & -L \sin \varphi \\ \sin \varphi & L \cos \varphi \end{pmatrix} \begin{pmatrix} \frac{r}{2} & \frac{r}{2} \\ \frac{r}{2l} & -\frac{r}{2l} \end{pmatrix}.$$

Since  $\det A(\varphi) = -\frac{Lr^2}{2l} \neq 0$ , it is clear that an input-output linearization scheme can be

proposed for  $(\omega_r, \omega_l) - (x_1, y_1)$ . According to [18], an input-output linearization control that allows the WMR to accomplish the obstacle avoidance task and reach the goal can be written as follows:

$$\begin{pmatrix} \omega_r \\ \omega_l \end{pmatrix} = \frac{v_d}{\sqrt{f_x^2 + f_y^2 + \varepsilon}} \frac{1}{Lr} \begin{pmatrix} L \cos \varphi - l \sin \varphi & l \cos \varphi + L \sin \varphi \\ L \cos \varphi + l \sin \varphi & - (l \cos \varphi - L \sin \varphi) \end{pmatrix} \begin{pmatrix} f_x \\ f_y \end{pmatrix}, \quad (13)$$

where  $v_d$  is a desired constant velocity,  $\varepsilon$  is a constant value close to zero, and  $f_x$  and  $f_y$  are the components of  $F_{total}$  in directions  $X$  and  $Y$ , respectively.

When there are  $n$  obstacles located within the workspace,  $f_x$  and  $f_y$  are determined by

$$\begin{pmatrix} f_x \\ f_y \end{pmatrix} = \begin{pmatrix} f_{xat} + f_{x1rep} + f_{x2rep} + \dots + f_{xnrep} \\ f_{yat} + f_{y1rep} + f_{y2rep} + \dots + f_{ynrep} \end{pmatrix}, \quad (14)$$

with  $f_{xat}$  the attractive force component associated with the goal in direction  $X$ , and  $f_{x1rep}, f_{x2rep}, \dots, f_{xnrep}$  the repulsive force components in direction  $X$  associated with obstacles  $1, 2, \dots, n$ , respectively. The description of the terms associated with  $f_y$  is highly similar to that for the terms associated with  $f_x$ .

Here we present the equations explicitly associated with (14) when it is supposed that, within the workspace, there are one and two obstacles, respectively.

- One obstacle:

In this situation, in accordance with (5) and (7), the attractive potential fields associated with the goal and its force components in directions  $X$  and  $Y$ , respectively, are given by

$$U_{at}(q) = \frac{1}{2} \zeta \left[ (x_1 - x_m)^2 + (y_1 - y_m)^2 \right], \quad (15)$$

$$f_{xat} = -\zeta(x_1 - x_m), \quad (16)$$

$$f_{yat} = -\zeta(y_1 - y_m). \quad (17)$$

Whereas, in accordance with (8) and (9), the repulsive potential fields associated with the obstacle and its force components in directions  $X$  and  $Y$ , respectively, are determined by

$$U_{1rep}(q) = \begin{cases} \frac{1}{2} \eta \left[ \frac{1}{\rho(q, q_{obs1})} - \frac{1}{\rho_{01}} \right]^2, & \text{for } \rho(q, q_{obs1}) \leq \rho_{01}, \\ 0, & \text{for } \rho(q, q_{obs1}) > \rho_{01}. \end{cases} \quad (18)$$

$$f_{x1rep} = \begin{cases} \eta \left[ \frac{1}{\rho(q, q_{obs1})} - \frac{1}{\rho_{01}} \right] \left[ \frac{1}{\rho^3(q, q_{obs1})} \right] (x_1 - x_{o1}), & \text{for } \rho(q, q_{obs1}) \leq \rho_{01}, \\ 0, & \text{for } \rho(q, q_{obs1}) > \rho_{01}. \end{cases} \quad (19)$$

$$f_{y1rep} = \begin{cases} \eta \left[ \frac{1}{\rho(q, q_{obs1})} - \frac{1}{\rho_{01}} \right] \left[ \frac{1}{\rho^3(q, q_{obs1})} \right] (y_1 - y_{o1}), & \text{for } \rho(q, q_{obs1}) \leq \rho_{01}, \\ 0, & \text{for } \rho(q, q_{obs1}) > \rho_{01}. \end{cases} \quad (20)$$

Therefore, for a scenario involving one obstacle, (14) is given by

$$\begin{pmatrix} f_x \\ f_y \end{pmatrix} = \begin{pmatrix} f_{x\text{at}} + f_{x1\text{rep}} \\ f_{y\text{at}} + f_{y1\text{rep}} \end{pmatrix}. \quad (21)$$

- Two obstacles:

The attractive force components associated with the goal,  $f_{x\text{at}}$  and  $f_{y\text{at}}$ , are determined by (16) and (17), respectively. Whereas the repulsive force components associated with one of the obstacles,  $f_{x1\text{rep}}$  and  $f_{y1\text{rep}}$ , are determined by (20) and (20), respectively, the second obstacle, which is associated with the repulsive potential field  $U_{2\text{rep}}(q)$ , has the following force components:

$$U_{2\text{rep}}(q) = \begin{cases} \frac{1}{2}\eta \left[ \frac{1}{\rho(q, q_{\text{obs}2})} - \frac{1}{\rho_{02}} \right]^2, & \text{for } \rho(q, q_{\text{obs}2}) \leq \rho_{02}, \\ 0, & \text{for } \rho(q, q_{\text{obs}2}) > \rho_{02}. \end{cases} \quad (22)$$

$$f_{x2\text{rep}} = \begin{cases} \eta \left[ \frac{1}{\rho(q, q_{\text{obs}2})} - \frac{1}{\rho_{02}} \right] \left[ \frac{1}{\rho^3(q, q_{\text{obs}2})} \right] (x_1 - x_{o2}), & \text{for } \rho(q, q_{\text{obs}2}) \leq \rho_{02}, \\ 0, & \text{for } \rho(q, q_{\text{obs}2}) > \rho_{02}. \end{cases} \quad (23)$$

$$f_{y2\text{rep}} = \begin{cases} \eta \left[ \frac{1}{\rho(q, q_{\text{obs}2})} - \frac{1}{\rho_{02}} \right] \left[ \frac{1}{\rho^3(q, q_{\text{obs}2})} \right] (y_1 - y_{o2}), & \text{for } \rho(q, q_{\text{obs}2}) \leq \rho_{02}, \\ 0, & \text{for } \rho(q, q_{\text{obs}2}) > \rho_{02}. \end{cases} \quad (24)$$

Thus, in a scenario two obstacles, (14) adopts the following expression:

$$\begin{pmatrix} f_x \\ f_y \end{pmatrix} = \begin{pmatrix} f_{x\text{at}} + f_{x1\text{rep}} + f_{x2\text{rep}} \\ f_{y\text{at}} + f_{y1\text{rep}} + f_{y2\text{rep}} \end{pmatrix}. \quad (25)$$

Finally, it is worth mentioning that for each obstacle present within the workspace there will exist a repulsive potential field; as a consequence, the terms associated with  $f_x$  and  $f_y$  will be increased depending on the number of obstacles.

### 3.2. DC motor control

In order to execute the obstacle avoidance task experimentally, the angular velocity profiles  $\omega_r$  and  $\omega_l$ , determined by the upper hierarchy (13), must be reproduced by the DC motors associated with the WMR prototype employed in the present work (see [14]). Thus for the right and left angular velocities of the DC motors to approach  $\omega_r$  and  $\omega_l$ , respectively, a PI controller is implemented for each motor.

A DC motor mathematical model expressed in terms of the motor shaft speed  $\omega$  is given by

$$\begin{aligned} L_a \frac{di_a}{dt} &= u - R_a i_a - k_e \omega, \\ J \frac{d\omega}{dt} &= -b\omega + k_m i_a, \end{aligned} \quad (26)$$

where  $u$  is the motor armature voltage,  $i_a$  is the armature current,  $k_e$  is the back-electromotive force constant,  $k_m$  is the motor torque constant,  $L_a$  is the armature inductance,  $R_a$  is the armature resistance,  $J$  is the rotor and load inertia, and  $b$  is the viscous friction constant due to both motor and load.

Since motor manufacturers do not generally provide all of the parameter values associated with (26), these values can be simply obtained via the reduction of (26) to a first order system that relates  $\omega$  to  $u$ . This is accomplished by assuming that  $L_a \approx 0$  in (26). Hence, the simplified model is determined by

$$\frac{d\omega}{dt} = -\alpha\omega + \beta u. \quad (27)$$

Characterization of  $\alpha$  and  $\beta$  associated with the prototype's DC motors –two Engel GNM3150s (24 V, 55 W) with G2.6 gearboxes– was previously carried out in [14]. In this latter study it was found that the simplified model (27) of the right and left motors can be respectively expressed by

$$\begin{aligned} \frac{d\omega_r}{dt} &= -10.20\omega_r + 5.51u_r, \\ \frac{d\omega_l}{dt} &= -10.20\omega_l + 5.99u_l, \end{aligned} \quad (28)$$

where  $\omega_r$  and  $\omega_l$  are the right and left angular velocity of the motors, and  $u_r$  and  $u_l$  represent the armature voltages of the right and left motors, respectively. Hence, a PI control for (27) that achieves  $\omega \rightarrow \omega^*$  is determined by

$$u = K_p e + K_i \int_0^t e d\tau, \quad (29)$$

with

$$e = \omega^* - \omega, \quad (30)$$

where  $e$  is the tracking error,  $\omega^*$  is the desired angular velocity trajectory,  $K_p$  is the proportional gain, and  $K_i$  is the integral gain. Next, (29) is applied to the DC motors of the WMR.

### 3.3. Hierarchical control

This subsection presents the connection of the control laws developed via a hierarchical control, a block diagram of which is shown in Figure 5. At the upper level, an input-output linearization control was used for the WMR model, generating the desired velocity profiles,  $\omega_r$  and  $\omega_l$ , for the robot wheels to track. These velocity profiles ensure that the WMR moves from the starting point to the goal point while avoiding the obstacles placed in between.

At the lower level, two PI controllers for the DC motors were considered, ensuring that the actual wheel velocities followed the desired velocity profiles generated at the upper level.

In accordance with (28), the mathematical models associated with the right and left motors are expressed as follows:

$$\begin{aligned} \frac{d\omega_r}{dt} &= -10.20\omega_r + 5.51u_r, \\ y_r &= \omega_r, \end{aligned} \quad (31)$$

and

$$\begin{aligned} \frac{d\omega_l}{dt} &= -10.20\omega_l + 5.99u_l, \\ y_l &= \omega_l. \end{aligned} \quad (32)$$

Thus, two controls,  $u_r$  and  $u_l$ , are required; in accordance with (29), these are given by

$$u_r = K_{pr}e_r + K_{ir} \int_0^t e_r d\tau, \quad (33)$$

$$u_l = K_{pl}e_l + K_{il} \int_0^t e_l d\tau, \quad (34)$$

where  $u_r$  and  $u_l$  are the control voltages for the right and left motors, respectively, and  $K_{pr}$ ,  $K_{ir}$ ,  $K_{pl}$ , and  $K_{il}$  are the constant gains (proportional and integral) associated with each motor. Finally,  $e_r$  and  $e_l$  represent the angular velocity tracking errors defined by

$$\begin{aligned} e_r &= \omega_r^* - \omega_r, \\ e_l &= \omega_l^* - \omega_l, \end{aligned} \quad (35)$$

with

$$(\omega_r^*, \omega_l^*) = (\omega_r, \omega_l). \quad (36)$$

This means that the desired angular velocity trajectories  $(\omega_r^*, \omega_l^*)$  are determined by  $(\omega_r, \omega_l)$ , which are obtained from (13).

## 4. Simulations

Using MATLAB-Simulink, which allows the programming of mathematical models by means of blocks that facilitate the establishment of equations in a transparent and simple manner, this section presents the numerical simulations associated with the obstacle avoidance task developed previously, with the general results then applied to a scenario involving three obstacles within the WMR workspace. As mentioned earlier, the positions of the obstacles

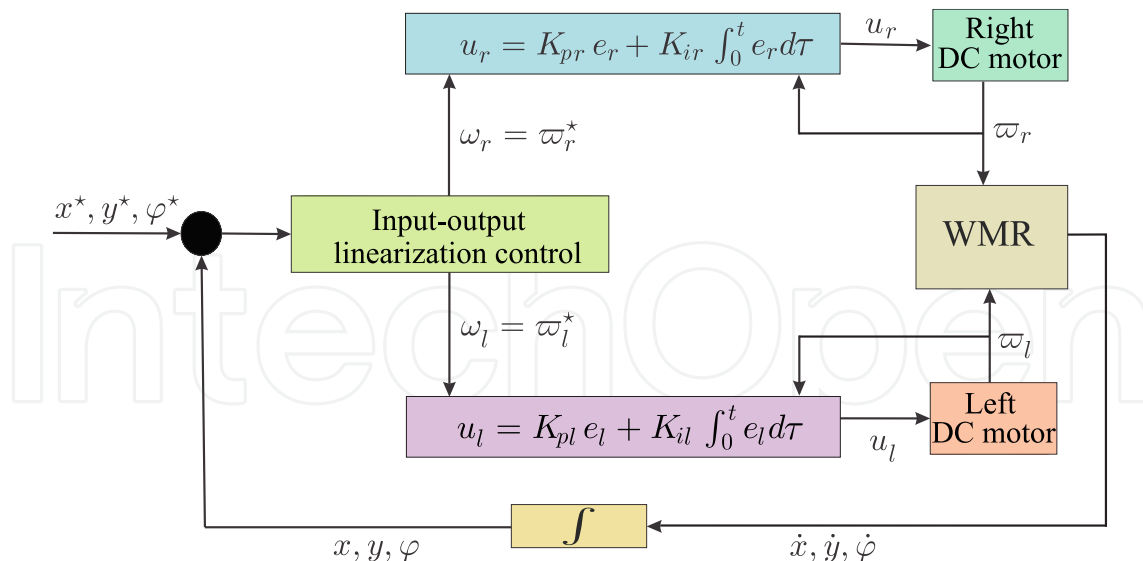


Figure 5. Block diagram of the WMR hierarchical control.

within the workspace is assumed to be already known. The following subsections outline the stages of the simulation process, namely: the definition of the parameters of the system and of the hierarchical control, the implementation of the control via MATLAB-Simulink, and finally the obtained results.

4.1. Definition of parameters

When implementing simulations associated with the closed-loop system, both WMR and control parameters must first be considered in order to use them later to program (via MATLAB-Simulink) the block associated with the hierarchical control. In this case, the parameters associated with the WMR are  $l$ ,  $r$ , and  $L$ , and those associated with the hierarchical control being  $v_d$ ,  $\varepsilon$ ,  $\eta$ ,  $\xi$ , and  $\rho_0$  due to the use of the artificial potential field method. The values of these parameters are shown in Table 1. It is worth mentioning that the values associated with the WMR, i.e.,  $l$ ,  $r$ , and  $L$ , correspond to the prototype reported in [14]. Finally, the coordinates associated with the goal,  $q_m$ , and the obstacles,  $q_{obs}$ , (for a three obstacle scenario) are presented in Table 2, where  $\rho_0 = \rho_{01} = \rho_{02} = \rho_{03}$ . The declarations elaborated in MATLAB-Simulink for all the above-mentioned parameters are shown in the upper part of Figure 6.

Constant	Definition	Value
$l$	Distance from $(x, y)$ to the wheels	0.220 m
$r$	Wheel ratio	0.075 m
$L$	Distance from $(x, y)$ to $q$	0.250 m
$v_d$	Desired constant velocity	0.5 m/s
$\varepsilon$	Constant value close to zero	0.1
$\eta$	Positive scale factor (repulsive)	2
$\xi$	Positive scale factor (attractive)	1
$\rho_0$	Distance of the obstacle's influence	0.5 m

Table 1. Parameters employed in the development of the simulations.

$q(x_1, y_1)$	$q_m(x_m, y_m)$	$q_{obs1}(x_{o1}, y_{o1})$	$q_{obs2}(x_{o2}, y_{o2})$	$q_{obs3}(x_{o3}, y_{o3})$
$x_1 = 0$ m	$x_m = 2.2$ m	$x_{o1} = 0.2$ m	$x_{o2} = 1.2$ m	$x_{o3} = 1.5$ m
$y_1 = 0$ m	$y_m = 1.7$ m	$y_{o1} = 0.4$ m	$y_{o2} = 0.4$ m	$y_{o3} = 1.6$ m
		$\rho_{o1} = 0.5$ m	$\rho_{o2} = 0.5$ m	$\rho_{o3} = 0.5$ m

**Table 2.** Coordinates associated with the goal and the obstacles.

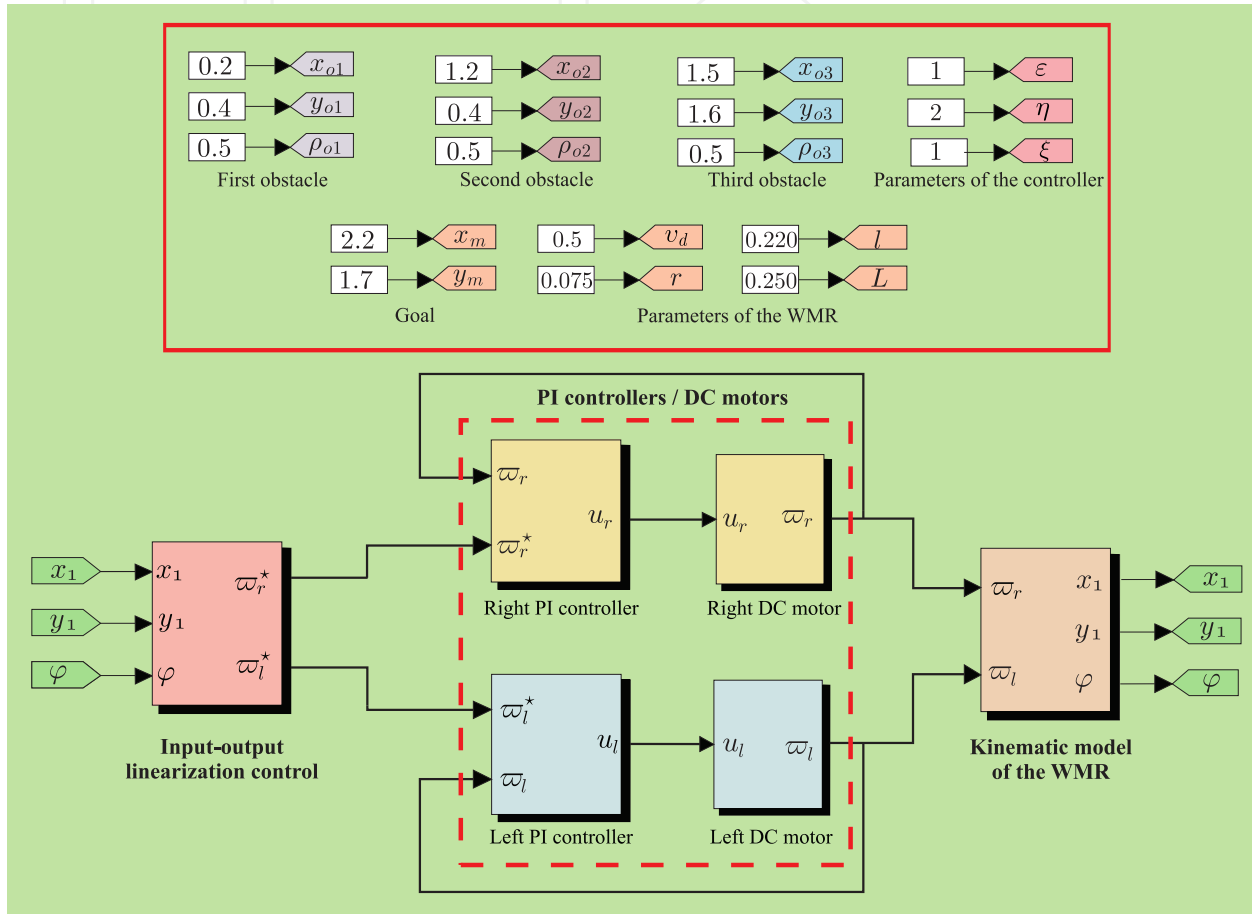


**Figure 6.** Implementation of the hierarchical control in MATLAB-Simulink for the WMR.

Once the values of the parameters associated with the WMR and the control have been defined, the hierarchical control can be programmed in MATLAB-Simulink to simulate the closed-loop system.

## 4.2. Implementing the control via MATLAB-Simulink

Figure 6 (bottom part) shows the three blocks associated with the hierarchical control programmed using MATLAB-Simulink: *Input-output linearization control*, *PI controllers/DC motors*, and *Kinematic model of the WMR*.

- 1.- *Input-output linearization control* block. In this block, the control determined by (13), which accomplishes the obstacle avoidance task, is programmed. The inputs are the variables  $(x_1, y_1, \varphi)$ , and the outputs the desired velocity profiles  $(\omega_r, \omega_l) = (\omega_r^*, \omega_l^*)$ , the latter

being tracked by the angular velocities of the right and left DC motors, respectively. Figure 7 presents the block's constituent sub-blocks.

- 2.- *PI controllers/DC motors* block. In this block, the PI controls, associated with the right and left motors, respectively determined by (33) and (34), are implemented. The inputs are determined by  $(\omega_r^*, \omega_l^*)$  and the angular velocities produced by the motors  $(\omega_r, \omega_l)$ , respectively, with the outputs being the controls  $u_r$  and  $u_l$  in such a way that  $(\omega_r, \omega_l) \rightarrow (\omega_r^*, \omega_l^*)$ . The gains associated with the PI controls were here selected as  $K_{pr} = 2$ ,  $K_{ir} = 50$ ,  $K_{pl} = 2$ , and  $K_{il} = 50$ .
- 3.- *Kinematic model of the WMR* block. In this block, the kinematic model of the WMR associated with the point  $q$ , determined by (12), is programmed. The inputs are  $(\omega_r, \omega_l)$ , and the outputs the variables  $(x_1, y_1, \varphi)$ .

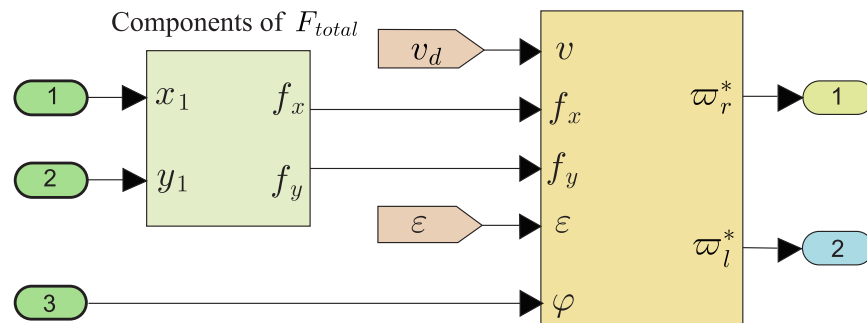


Figure 7. Input-output linearization control block.

### 4.3. Simulation results

Finally, this subsection presents the simulation results associated with the obstacle avoidance task for the differentially-driven WMR. The simulations consider the presence of three obstacles within the workspace which have an influence over the WMR during its journey to the goal. Table 2 presents the coordinates associated with the goal and the three obstacles, with the distribution depicted in Figure 8(a) and Figure 14. The results obtained for the variables of interest to the WMR are shown in Figure 8; in this figure one can observe how the WMR successfully evades the obstacles and reaches the goal.

## 5. Description of the employed prototype

This section provides a general description of the WMR prototype reported in [14], which was built to carry out various control tasks associated with WMRs. Figure 9 displays a block diagram describing the existent connections between the different stages of the employed WMR, namely: *Subsystems*, *Power system*, and *Data acquisition and control system*.

Here we present a summarized description of the blocks composing the WMR prototype, including its connection with the DS1104 board, as shown in Figure 9.

- Stage 1: *Subsystems*. This stage (see Figure 10) comprises the mechanical subsystems **a** and **b**, which include the actuators, sensors, and the mechanical structure of the WMR. Subsystem **a**, *actuators and sensors*, generates the movement of the WMR wheels in a specified workspace, and discrete position sensing, respectively. Subsystem **b**, *mechanical*

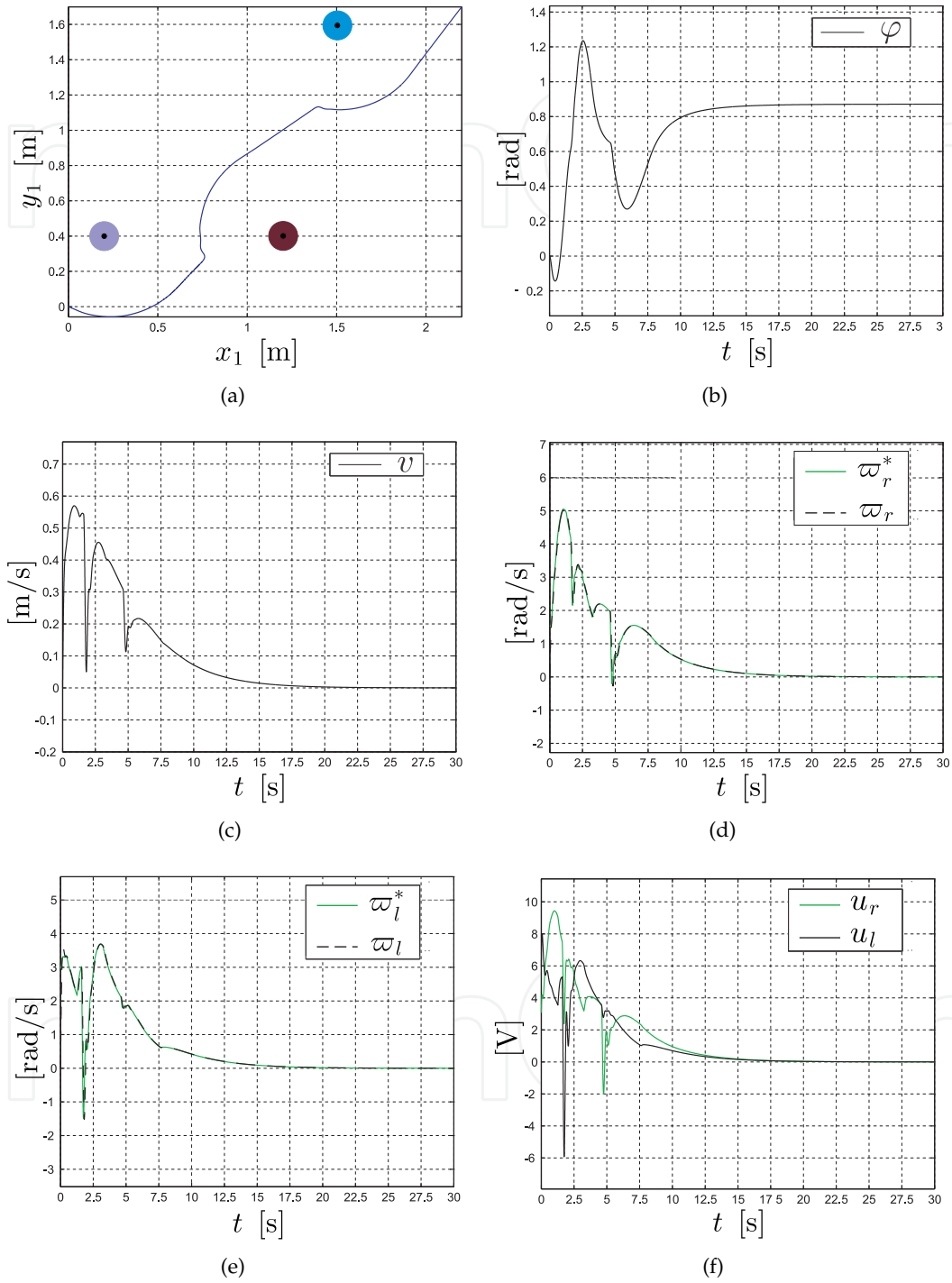


**Figure 8.** Simulation results in the three obstacles scenario.

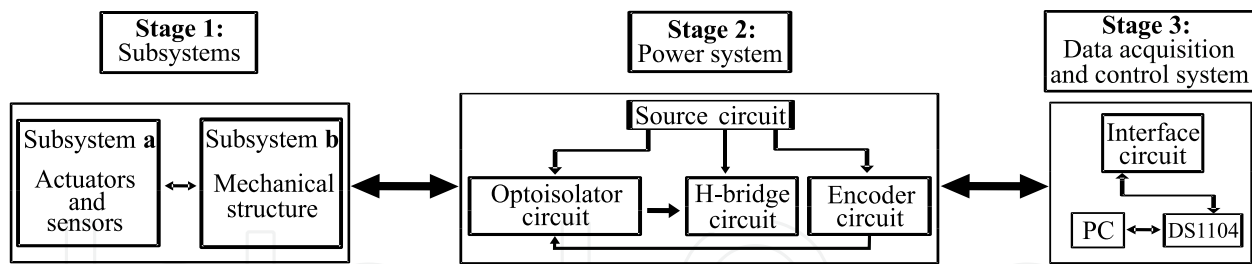


**Figure 9.** General block diagram of the WMR prototype.

*structure*, corresponds to the mechanical topology associated with the differentially driven WMR.

- **Stage 2: Power system.** This stage enables interaction between the electronic control interface (stage 3) and the mechanical subsystems (stage 1). A block diagram of stage 2 is shown in Figure 11. This block comprises the following four substages, numbered from 1 to 4: *source circuit*, *optoisolator circuit*, *H-bridge circuit*, and *encoder circuit*. In substage 1, the power supply, via the source circuit, distributes the different voltages to the general electronic system. Substage 2 enables electrical signal isolation between the DS1104 electronic board and substage 3. Substage 3 enables the direction of rotation of the DC motors to be controlled via the use of a positive or a negative voltage, which is determined by the control exerted by the DS1104 board. Finally, substage 4 involves the acquisition of the encoders' signals, which can then be used to estimate the position of the WMR within the workspace.
- **Stage 3: Data acquisition and control system.** The main device involved in this stage is the DS1104 board, which performs the acquisition of the variables of interest to the experimental implementation of the WMR hierarchical control. This board was selected due to the potential for integration between MATLAB-Simulink and the board's firmware. Moreover, the high programming level available in Simulink makes it a practical selection for the programming of complex control strategies in a graphical environment. Stage 3 also includes an *interface circuit* (see Figure 9) which establishes communication between the DS1104 board and the WMR.

Figure 12 shows pictures of the real WMR, including the employed instrumentation.

## 6. Real-time experiments

In order to validate the data obtained via numeric simulation presented in Section 4, here we present the experimental results obtained using the WMR in real-time. These experiments were performed using MATLAB-Simulink, ControlDesk, and a DS1104 board (dSPACE), with the distribution of the obstacles and the goal identical to that in the simulations.

### 6.1. Real-time control of the WMR via MATLAB-Simulink

Whereas the mathematical models associated with the WMR and the DC motors were used to obtain the simulation results, these models were replaced by the WMR prototype in obtaining the experimental results. However, it is worth mentioning that the robot kinematic model

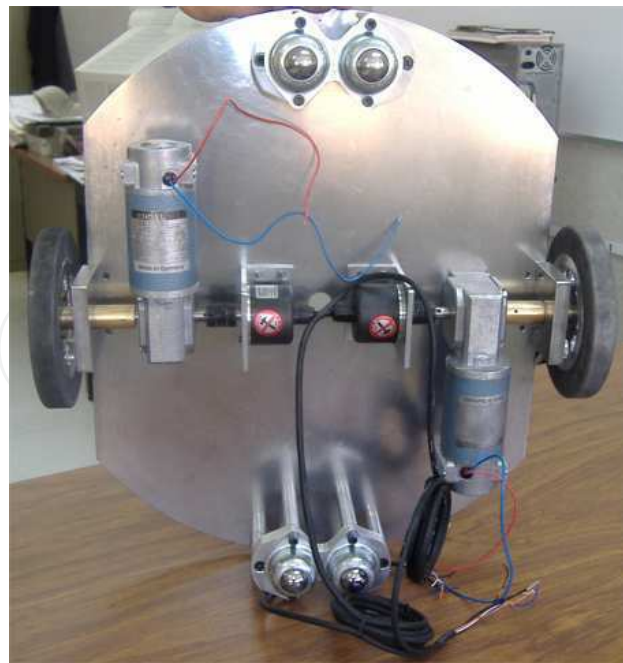


**Figure 10.** Bottom view of the mechanical structure.

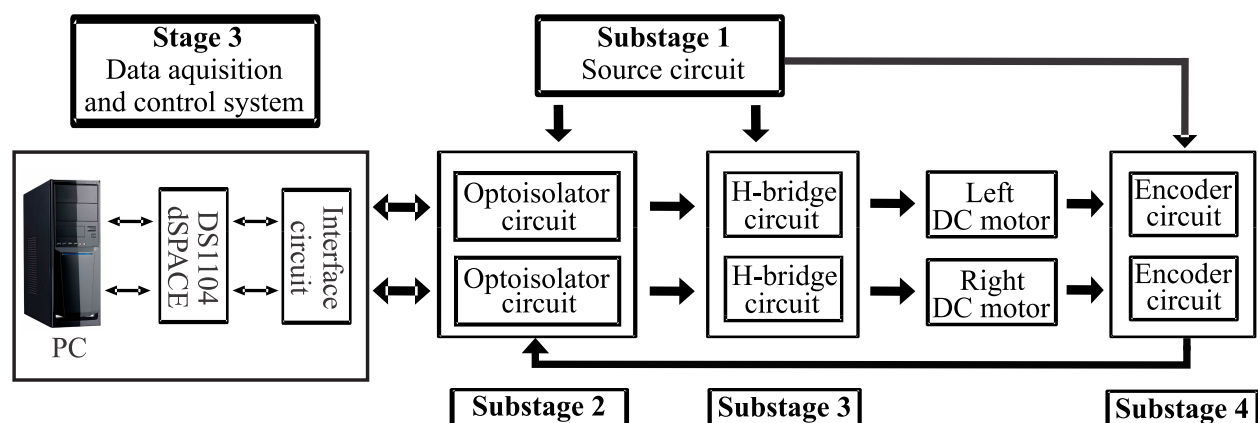


**Figure 11.** Block diagram of the power system.

was employed here to provide an estimation of the WMR position, since no localization sensor was used for the WMR in the present study.

The MATLAB-Simulink program associated with the hierarchical control used to obtain the experimental results for the closed-loop system is shown in Figure 13, which consists of the following blocks: *System parameters*, *Input-output linearization control*, *PI controllers/DC motors*, and *Kinematic model of the WMR*. Figure 13 also depicts the connections between the WMR and the hierarchical control. A comparison of Figures 6 and 13 reveals that the two are highly similar, with the only block experiencing any significant changes being the one associated with the *PI controllers/DC motors*. Hence, we can focus our attention solely on this block.

- *PI controllers/DC motors* block. This block describes the implementation of the PI controls,  $u_r$  and  $u_l$ , associated with the right and left motors, respectively, which allow  $(\omega_r, \omega_l) \rightarrow$

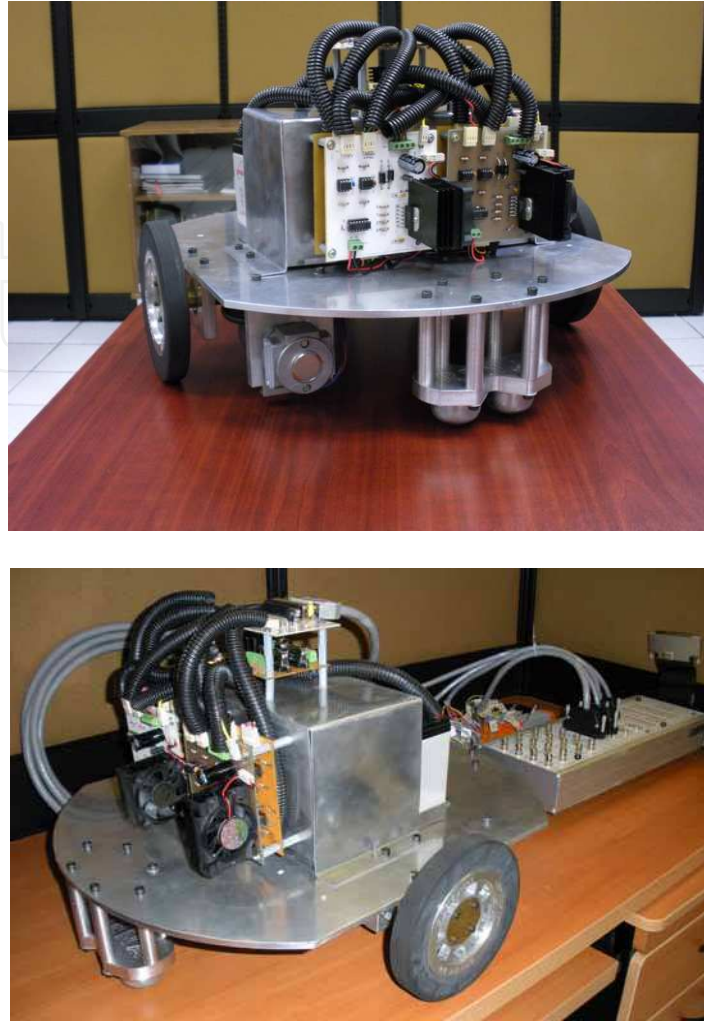


**Figure 12.** WMR prototype.

$(\omega_r^*, \omega_l^*)$ . In order to start the DC motors, the  $u_r$  and  $u_l$  voltages must be conditioned through PWM blocks, which are implemented via the DS1104 board. The PWM signals then go through the *power system* stage illustrated in Figure 9. For the acquisition of the angular velocities  $\omega_r$  and  $\omega_l$ , two E50S8 incremental encoders (Autonics) were employed in combination with MATLAB-Simulink blocks.

## 6.2. Experimental results

This subsection presents the experimental results associated with the distribution of the obstacles and the goal mentioned in Table 2. Likewise, the locations of the WMR, obstacles, and goal within the workspace are illustrated in Figure 14. The corresponding experimental results for such a scenario, in which the parameters of the WMR and the gains of the controls were the same as those employed in the simulations, are shown in Figure 15. Additionally, supplementary material associated with these results can be seen through Video S1 (see [25]). Also, experimental results for the scenarios involving two and zero obstacles within

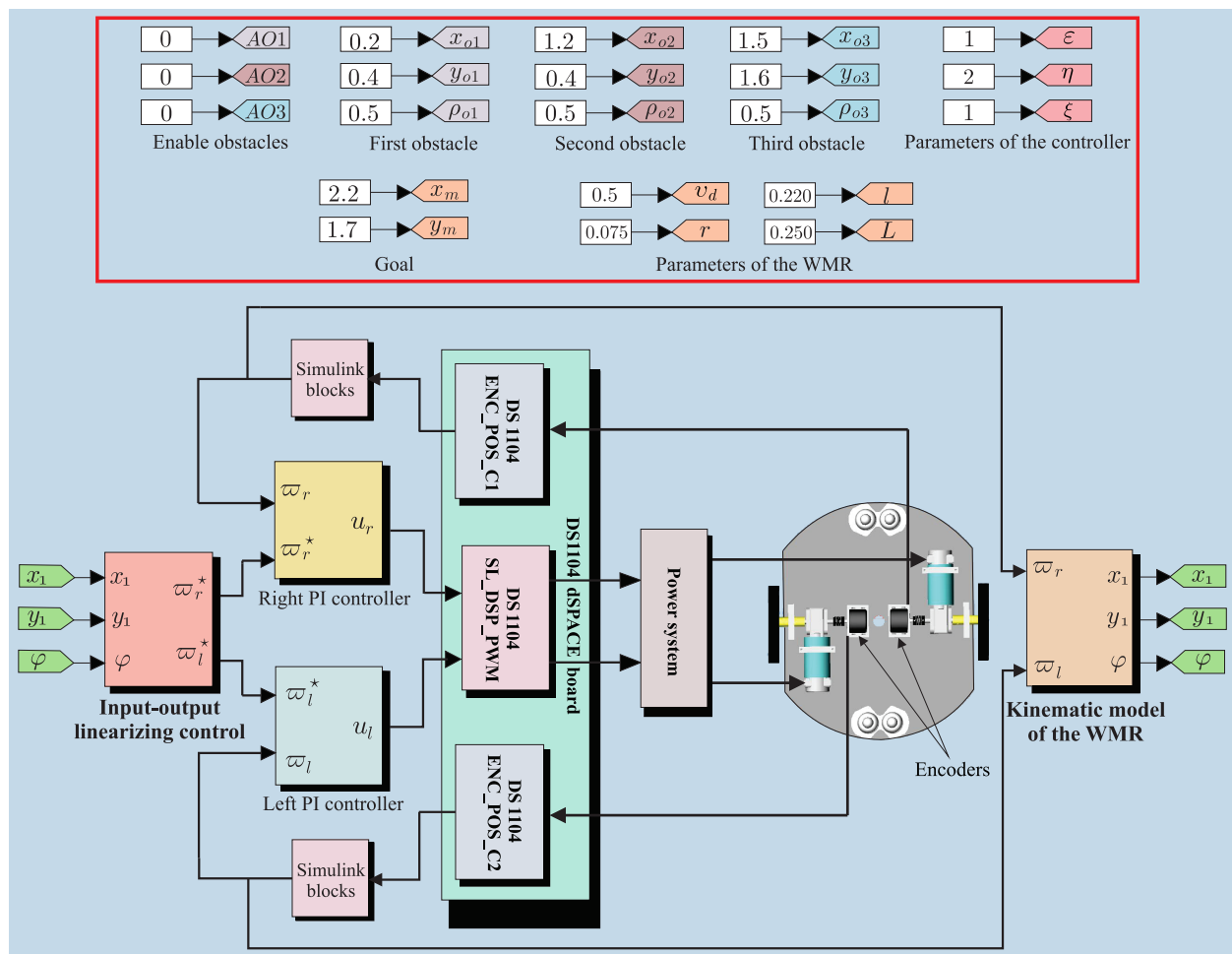


**Figure 13.** Experimental implementation of the controller via MATLAB-Simulink and its connection with the WMR.

the workspace are presented in Videos S2 and S3, respectively, (see [25]). The aforementioned videos are available online at: [www.controlautomatico.com.mx/trabajos.html](http://www.controlautomatico.com.mx/trabajos.html)

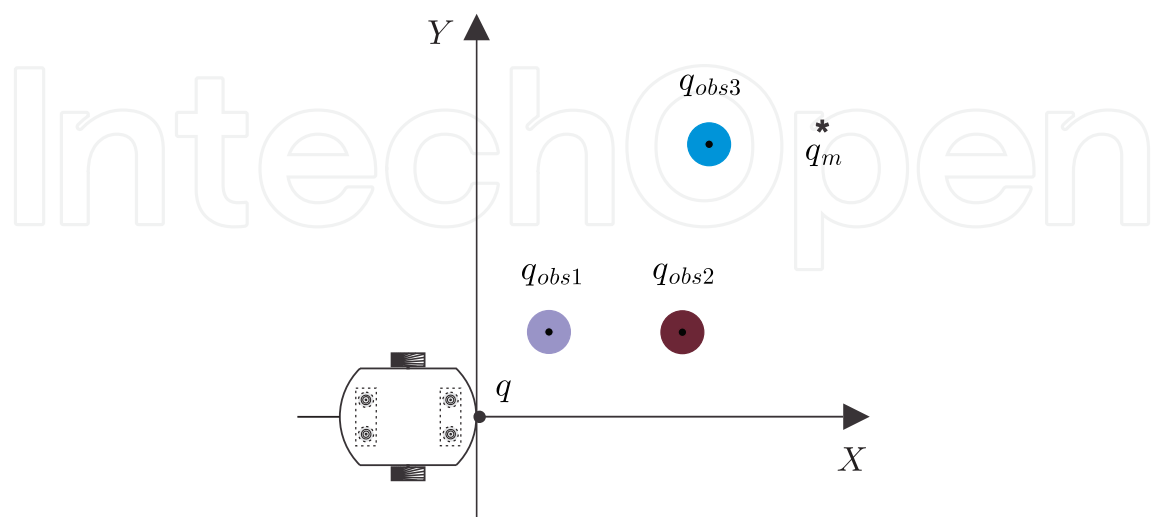


**Figure 14.** Position and orientation of the starting point of the WMR.

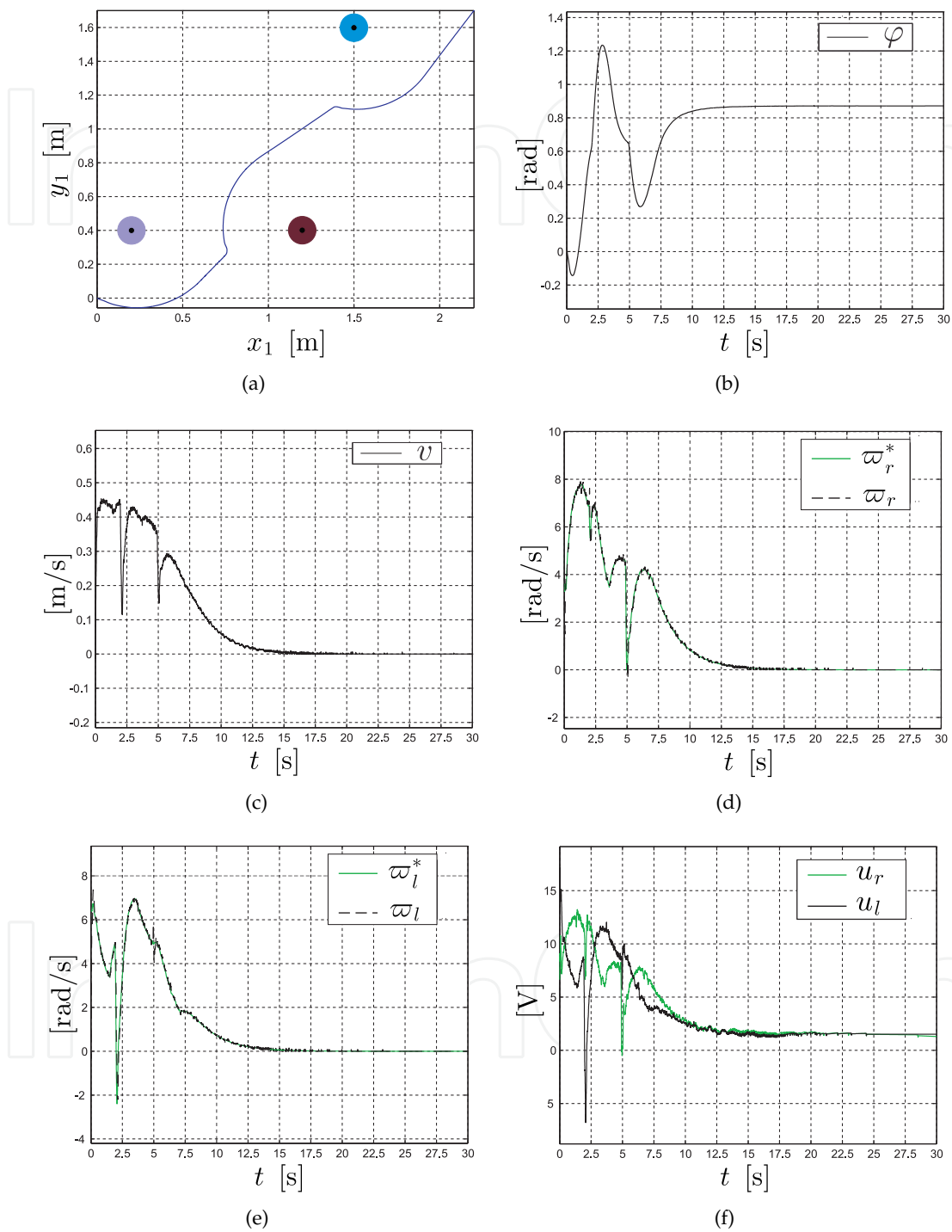


**Figure 15.** Experimental results for the three obstacles scenario.

### 6.3. Discussion of the results

Similar results were obtained in the simulation and experimental tests; in both cases the angular velocities of the DC motors,  $\omega_r$  and  $\omega_l$ , tracked the desired velocity profiles imposed by the WMR kinematic model,  $\omega_r^*$  and  $\omega_l^*$ , respectively. Hence, the obstacle avoidance task was successfully carried out by the WMR, as verified experimentally in Figure 15(a). However, it is worth mentioning that an error arose that could only be appreciated visually and which thus does not appear in Figure 15(a): a gap of approximately 10 cm was observed between point  $q$  and point  $q_m$ . This discrepancy likely occurred due to the fact that the position of  $q$  within the workspace was calculated indirectly via the WMR kinematic model. It was also observed that the voltages  $u_r$  and  $u_l$ , associated with the DC motors, did not surpass the  $(-24 \text{ V}, +24 \text{ V})$  voltage interval: this was convenient since the nominal voltage of the employed DC motors is in the range of  $\pm 24 \text{ V}$ . As a result it can be confirmed that the developed hierarchical control performed successfully.

## 7. Conclusions

Based on the artificial potential field approach, the present work has provided a solution to the obstacle avoidance task for a differentially-driven WMR via the design of a hierarchical control, for which a step-by-step guide has been presented that details the theory, simulation, and experimental implementation. Simulation results were obtained by developing a MATLAB-Simulink program, since Simulink provides a graphical environment that facilitates the analysis, design, and construction of dynamic systems. In order to obtain experimental results, a MATLAB-Simulink program was again employed, this time alongside ControlDesk and the DS1104 board. A comparison of the simulation and experimental results associated with the obstacle avoidance task revealed the good performance of the developed hierarchical control. However, as mentioned earlier, an error between the WMR and the goal arises that can only be observed visually, likely due to the fact that the position of the robot is calculated via the kinematic model of the WMR. Future work will aim to locate the WMR via a sensor in order to reduce or eliminate said error.

## Acknowledgments

R. Silva-Ortigoza, H. Taud, M. Marciano-Melchor, and J. A. Álvarez-Cedillo acknowledge financial support from the Secretaría de Investigación y Posgrado del Instituto Politécnico Nacional (SIP-IPN), SNI-México, and the IPN programs EDI and COFAA. The work of C. Márquez-Sánchez was supported by CONACYT and BEIFI scholarships. V. M. Hernández-Guzmán acknowledges financial support from SNI-México. Finally, Rhomina and Joserhamón deserve a special mention from R. Silva-Ortigoza for their moral support and for being the inspiration for his introduction to the thrilling world of robotics.

## Author details

R. Silva-Ortigoza<sup>1</sup>, C. Márquez-Sánchez<sup>1</sup>, F. Carrizosa-Corral<sup>2</sup>, V. M. Hernández-Guzmán<sup>3</sup>, J. R. García-Sánchez<sup>1</sup>, H. Taud<sup>1</sup>, M. Marciano-Melchor<sup>1</sup>, and J. A. Álvarez-Cedillo<sup>1</sup>

1 Instituto Politécnico Nacional, CIDETEC, Área de Mecatrónica, Unidad Profesional Adolfo López Mateos, México, DF, Mexico

2 Instituto Tecnológico de Culiacán, Departamento de Metal-Mecánica, Culiacán, Sin, Mexico

3 Universidad Autónoma de Querétaro, Facultad de Ingeniería, Querétaro, Qro, Mexico

## References

- [1] R. Silva-Ortigoza, M. Marcelino-Aranda, G. Silva-Ortigoza, V. M. Hernández-Guzmán, M. A. Molina-Vilchis, G. Saldaña-González, J. C. Herrera-Lozada, and M. Olguín-Carbajal, "Wheeled mobile robots: A review," *IEEE Latin America Transactions*, vol. 10, no. 6, pp. 2209–2217, 2012. Available at <http://www.ewh.ieee.org/reg/9/etrans/eng/>
- [2] J. L. Crowley, "World modeling and position estimation for a mobile robot using ultrasonic rangin," in *Proceedings of the IEEE International Conference on Robotics and Automation*, pp. 674–680, May 1989.
- [3] J. T. Schwartz and M. Sharir, "On the piano movers problem. II. General techniques for computing topological properties of real algebraic manifolds," *Advances in Applied Mathematics*, vol. 4, no. 3, pp. 298–351, 1983.
- [4] N. J. Nilsson, "A mobile automaton: An application of artificial intelligence techniques," in *Proceedings of the International Joint Conference on Artificial Intelligence*, pp. 509–520, May 1969.
- [5] O. Khatib, "Real-Time obstacle avoidance for manipulators and mobile robots, " *The international Journal of Robotics Research*, vol. 5, no. 2, pp. 90–98, 1986.
- [6] J. Borenstein and Y. Koren, "Obstacle avoidance with ultrasonic sensors," *IEEE Journal of Robotics and Automation*, vol 4, no. 2, pp. 213–218, 1988.
- [7] J. Borenstein and Y. Koren, "Real-Time obstacle avoidance for fast mobile robots, " *IEEE Transactions on Systems, Man and Cybernetics*, vol. 19, no. 5, pp. 1179–1187, 1989.
- [8] R. Tilove, "Local obstacle avoidance for mobile robots based on the method of artificial potentials," in *Proceedings of the IEEE International Conference on Robotics and Automation*, pp. 566–571, May 1990.
- [9] J. Borenstein and Y. Koren, "Potential field methods and their inherent limitations for mobile robot navigation," in *Proceedings of the IEEE International Conference on Robotics and Automation*, pp. 1398–1404, April 1991.
- [10] J. Guldner and V. I. Utkin, "Sliding mode control for gradient tracking and robot navigation usig artificial potential fields," *IEEE Transactions on Robotics and Automation*, vol. 11, no. 2, pp. 247–254, 1995.

- [11] K. Valanavis, T. Hebert, R. Kolluru, and N. Tsourveloudis, "Mobile robot navigation in 2-D dynamic environments using an electrostatic potential field," *IEEE Transactions on Systems, Man and Cybernetics, Part A: Systems and Humans*, vol. 30, no. 2, pp. 187–196, 2000.
- [12] F. Xu, H. Van Brussel, M. Nuttin, and R. Moreas, "Concepts for dynamic obstacle avoidance and their extended application in underground navigation," *Robotics and Autonomous Systems*, vol. 42, no. 1, pp. 1–15, 2003.
- [13] W. Huang, B. Fajen, J. Fink, and W. Warren, "Visual navigation and obstacle avoidance using a steering potential function," *Robotics and Autonomous Systems*, vol. 54, no. 4, pp. 288–299, 2006.
- [14] R. Silva-Ortigoza, C. Márquez-Sánchez, M. Marcelino-Aranda, M. Marciano-Melchor, G. Silva-Ortigoza, R. Bautista-Quintero, E. R. Ramos-Silvestre, J. C. Rivera-Díaz, and D. Muñoz-Carrillo, "Construction of a WMR for trajectory tracking control: Experimental results," *The Scientific World Journal*, vol. 2013, Article ID 723645, pp. 1–17, 2013. Available at <http://dx.doi.org/10.1155/2013/723645>
- [15] V. M. Hernández-Guzmán, R. Silva-Ortigoza y R. V. Carrillo-Serrano, *Control Automático: Teoría de Diseño, Construcción de Prototipos, Modelado, Identificación y Pruebas Experimentales*, Colección CIDETEC-IPN, Mexico, DF, Mexico, 2013. Available at <http://www.controlautomatico.com.mx>
- [16] S. S. Ge and Y. J. Cui, "New potential functions for mobile robot path planning," *IEEE Transactions on Robotics and Automation*, vol. 16, no. 5, pp. 615–620, 2000.
- [17] B. H. Krogh, "A generalized potential field approach to obstacle avoidance control," *International Robotics Research Conference*, Bethlehem, PA, August 1984.
- [18] J. R. García Sánchez, *Diseño y construcción de un robot móvil, aplicando el método de campos potenciales en la evasión de obstáculos*. Tesis de Maestría. CIDETEC del Instituto Politécnico Nacional, Mexico City, Mexico, 2008.
- [19] A. W. Divelbiss and J. T. Wen, "Trajectory tracking control of a car-trailer system," *IEEE Transactions on Control Systems Technology*, vol. 5, no. 3, pp. 269–278, 1997.
- [20] R. Silva-Ortigoza, G. Silva-Ortigoza, V. M. Hernández-Guzmán, V. R. Barrientos-Sotelo, J. M. Albarrán-Jiménez, and V. M. Silva-García, "Trajectory tracking in a mobile robot without using velocity measurements for control of wheels," *IEEE Latin America Transactions*, vol. 6, no. 7, pp. 598–607, 2008. Available at <http://www.ewh.ieee.org/reg/9/etrans/eng/>
- [21] R. Silva-Ortigoza, J. R. García-Sánchez, J. M. Alba-Martínez, V. M. Hernández-Guzmán, M. Marcelino-Aranda, H. Taud, and R. Bautista-Quintero, "Two-stage control design of a Buck converter/DC motor system without velocity measurements via a  $\Sigma - \Delta$ -modulator," *Mathematical Problems in Engineering*, vol. 2013, Article ID 929316, pp. 1–11, 2013. Available at <http://dx.doi.org/10.1155/2013/929316>

- [22] R. Silva-Ortigoza, C. Márquez-Sánchez, F. Carrizosa-Corral, M. Antonio-Cruz, J. M. Alba-Martínez, and G. Saldaña-González, "Hierarchical velocity control based on differential flatness for a DC/DC Buck converter-DC motor System," *Mathematical Problems in Engineering*, vol. 2014, Article ID 912815, pp. 1–12, 2014. Available at <http://dx.doi.org/10.1155/2014/912815>
- [23] R. Silva-Ortigoza, V. M. Hernández-Guzmán, M. Antonio-Cruz, and D. Muñoz-Carrillo, "DC/DC Buck power converter as a smooth starter for a DC motor based on a hierarchical control," *IEEE Transactions on Power Electronics*, Article in Press, Available with DOI: 10.1109/TPEL.2014.2311821
- [24] H. Sira-Ramirez and S. K. Agrawal, *Differentially Flat Systems*, Marcel Dekker, New York, 2004.
- [25] Supplementary Material. Available at <http://www.controlautomatico.com.mx/trabajos.html>
- [26] T. A. Vidal Calleja, *Generalización del método de campos potenciales artificiales para un vehículo articulado*. Tesis de Maestría. Sección de Mecatrónica del Departamento de Ingeniería Eléctrica del CINVESTAV-IPN, Mexico City, Mexico, 2002.

IntechOpen